Journal of Environmental Chemical Engineering 10 (2022) 107951

Contents lists available at ScienceDirect

Journal of Environmental Chemical Engineering

journal homepage: www.elsevier.com/locate/jece

Aging studies on dual function materials Ru/Ni-Na/Ca-Al_2O_3 for CO_2 adsorption and hydrogenation to CH_4

Alejandro Bermejo-López, Beñat Pereda-Ayo, Jon A. Onrubia-Calvo, José A. González-Marcos, Juan R. González-Velasco *

Department of Chemical Engineering, Faculty of Science and Technology, Universidad del País Vasco UPV/EHU, Barrio Sarriena, s/n, 48940 Leioa, Bizkaia, Spain

ARTICLE INFO

Editor: Ana Loncaric Bozic

Keywords:
CO_2 hydrogenation
Integrated CO_2 capture and utilization
Methanation
Dual function material
Aging
Ru and Ni catalysts

ABSTRACT

Integrated CO_2 capture and utilization (ICCU) is a promising alternative to revalue CO_2. In this work, the influence of the aging process on dual function materials (DFMs) Ru/Ni-Na/Ca-Al_2O_3, for the conversion of CO_2 into CH_4 is studied. DFMs are characterized by N_2 adsorption-desorption, XRD, H_2 chemisorption, TEM and CO_2-TPD. The catalytic behavior of the prepared DFMs is analyzed in consecutive cycles of CO_2 adsorption and hydrogenation to CH_4. The aging process notably limits the physicochemical properties, especially the metallic dispersion. However, the CH_4 production decrease is less than 25% for aged Ru-DFMs, which makes them suitable for long-term operation. The aged DFM 4Ru-8Na_2CO_3/8CaO-Al_2O_3, presents a CH_4 production greater than 275 μmol g^{-1} with high selectivity in the range 340–400 °C. On the other hand, the aging process is more noticeable for Ni-DFMs; in fact, it limits the CH_4 production to half compared to reduced Ni-DFMs.

1. Introduction

Greenhouse gas emissions need to be reduced drastically to meet the Paris Agreement's climate objectives of limiting global average temperature increase below 2 °C and pursuing efforts limiting it to 1.5 °C [1,2]. This will require energy systems that differ much from today. Since industrial practices will depend on non-renewable sources for a relatively long time before there is a drastic shift to renewable energy, capture of produced CO_2 emerges as transit solution up to that date [3]. Once the CO_2 is captured, it can be stored (CCS) or used (CCU). At this point, creating a sustainable market demanding recovered CO_2 may provide a better option than CCS, while also helping the economy [4,5]. Specifically, research is shifting towards CO_2 capture and utilization (CCU). So that, the use of CO_2 in the synthesis of value-added products is increasing the attention of several industrial companies [6].

Recently, to avoid energy penalties associated with the regeneration and compression steps required for transportation and storage prior to conversion, researchers have attempted to integrate the CO_2 capture and utilization (ICCU) [7]. In this context, the CO_2 is captured and converted at the same place using dual function materials (DFMs). The DFMs consist of CO_2 adsorbents and catalytic phases. First, DFMs capture CO_2 from flue gas (4–14 vol% CO_2) to effectively reduce carbon emissions. When the carbon capture process is completed, the feed gas is switched to a reducing renewable agent for the conversion of the adsorbed CO_2 to synthetic fuels. An interesting option is the conversion of the adsorbed CO_2 into CH_4 through the Sabatier reaction (Eq. 1).

$$CO_2 + 4\ H_2 \leftrightarrows CH_4 + 2\ H_2O \quad (1)$$

Duyar et al. [8] in 2015 published the first work of the operation in cycles of CO_2 adsorption and hydrogenation to CH_4. The authors used a DFM based on CaO as adsorbent, Ru as metal phase and Al_2O_3 as support. They demonstrated the possibility of producing CH_4 from CO_2 adsorbed in an earlier step. From then, publications on cycles of CO_2 adsorption and hydrogenation to CH_4 is growing exponentially [7,9–11]. In general, DFMs are a combination of a compound based on Na [12,13], Ca [8,14], Mg [15,16] or K [15,17], as adsorbent, and a Ru- [12,18], Ni- [17,19] or Rh-based [20] as catalytic phase. Both phases are commonly supported on a high surface area carrier. Specifically, γ-Al_2O_3 is proposed as the best support [21].

One of the problems of the CO_2 methanation reaction is its highly exothermal character [22]. Therefore, it leads to a demand for highly thermostable catalysts to resist deactivation phenomena caused by hotspot formation in industrial fixed-bed application [23]. This problem is highly relevant in methanation with continuous feeding of CO_2 and H_2. In the operation in cycles of CO_2 adsorption and hydrogenation to CH_4, the temperature control is easier. Nevertheless, the main

* Corresponding author.
E-mail address: juanra.gonzalezvelasco@ehu.eus (J.R. González-Velasco).

https://doi.org/10.1016/j.jece.2022.107951
Received 7 February 2022; Received in revised form 5 May 2022; Accepted 18 May 2022
Available online 21 May 2022

deactivation phenomenon in the dual operation is the presence of oxygen and steam in the feed stream of the adsorption period, which influence has been analysed by several authors [21,24–26]. The presence of O_2 partially oxidizes the metal phase, which is reduced again during the hydrogenation period. On the other hand, the presence of H_2O reduces the CO_2 adsorption capacity due to competitive adsorption of both compounds over the same basic sites.

Another way to analyse the resistance of the DFMs to the presence of O_2 and steam is to age the DFMs at high temperature in the presence of O_2 and steam. This strategy is commonly used for NSR or SCR catalysts for NO_x removal in diesel vehicle engines [27–29]. In this way, the state of the catalyst at the end of the life of the vehicle can be simulated at a laboratory scale. In order to simulate long periods of DFM operation in cycles, with the presence of oxygen and steam during the adsorption period, the analysis of aged DFMs can be of great interest. The evaluation of the activity of the DFMs after being subjected to the aging protocol, as well as their physicochemical properties, will provide valuable information on their resistance to aging. However, to the best of our knowledge, the study of the resistance to hydrothermal aging in the presence of oxygen of DFMs has not yet been reported.

In this work, the effect of hydrothermal aging in the presence of oxygen on DFMs is analysed. Changes that are caused in their physicochemical properties are studied, as well as its influence in the activity in cycles of CO_2 adsorption and hydrogenation to CH_4. To have a broad view of the effect of aging, DFMs with different formulations are studied. With that aim, DFMs based on ruthenium, nickel or both as metals and on sodium, calcium or both as adsorbents are selected.

2. Experimental

2.1. DFM preparation

Five DFMs have been selected based on ruthenium, nickel or the combination of both as active metals, whereas sodium, calcium or the combination of both are used as adsorbents. Table 1 lists the complete formulation of DFMs prepared and their nomenclature used in this work, also classified into Ru-DFMs or Ni-DFMs group. Ru-DFMs with single-Na and single-Ca have been chosen, both with comparable activity [12]. In addition, a Ru-DFM with both adsorbents jointly (Na and Ca) is also studied, as it has recently been shown that this combination improves activity [30]. On the other hand, in the case of Ni-DFMs only Na is used as adsorbent, due to its significant higher activity as Ni-DFMs with Ca [14].

The DFMs were prepared by wetness impregnation. Firstly, appropriated amount of $Ca(NO_3)_2.4\ H_2O$ (*Merk*) and/or Na_2CO_3 (*Riedel de-Haën*) was impregnated over γ-Al_2O_3 (*Saint Gobain*). The impregnated powder was dried at 120 °C overnight. Then the powder was calcined at 400 °C (Ru-DFMs) or 550 °C (Ni-DFMs) for 4 h (1 °C min^{-1}). Afterwards, $Ru(NO)(NO_3)_2$ (*Sigma Aldrich*) and/or $Ni(NO_3)_2.6\ H_2O$ (*Fluka*) was impregnated over the previous calcined powder. After drying at 120 °C, the samples were stabilized by calcining again at the same conditions.

2.2. Reduction protocol

The calcined DFMs were placed in their granulated form (0.3–0.5 mm) in a quartz tube reactor and were heated rom RT to 400 °C (Ru-DFMs) or 500 °C (Ni-DFMs) at 10 °C min^{-1} during 1 h under 10% H_2/Ar (50 cm^3 min^{-1}).

Table 1
Nomenclature and group of the synthesized DFMs.

DFM	Nomenclature	Group
4%Ru-16%Na_2CO_3/γ-Al_2O_3	4Ru-16Na	Ru-DFM
4%Ru-8%Na_2CO_3-8%CaO/γ-Al_2O_3	4Ru-8Na/8Ca	Ru-DFM
4%Ru-16%CaO/γ-Al_2O_3	4Ru-16Ca	Ru-DFM
10%Ni-16%Na_2CO_3/γ-Al_2O_3	10Ni-16Na	Ni-DFM
1%Ru-10%Ni-16%Na_2CO_3/γ-Al_2O_3	1Ru/10Ni-16Na	Ni-DFM

2.3. Aging procedure

For hydrothermal aging studies in the presence of oxygen, the DFMs were placed in their granulated form (0.3–0.5 mm) in a quartz tube reactor placed in a horizontal furnace. The DFMs were aged under 5% H_2O and 5% O_2 in Ar for 3 h, at a total flow rate of 550 ml min^{-1}. The temperature for the aging procedure was 400 °C for Ru-DFMs and 550 °C for Ni-DFMs.

2.4. X ray diffraction (XRD)

X-ray diffraction spectra were obtained in a *Philips PW1710* diffractometer. The DFMs were finely ground and were subjected to Cu Kα radiation in a continuous scan mode from 5° to 70° 2θ with 0.02 per second sampling interval.

2.5. N_2 adsorption-desorption

Textural properties of the DFMs were determined from N_2 adsorption-desorption isotherms measured at − 196 °C using a *Micromeritics TRISTAR II 3020* instrument. Pore volumes were calculated by t-plot method while pore size distribution of mesoporous solids was determined using BJH method. The samples were pre-purged with nitrogen for 10 h at 300 °C using *SmartPrep degas system* (*Micromeritics*).

2.6. H_2 chemisorption

The dispersion of active metal sites was measured by H_2 chemisorption using a *Micromeritics ASAP 2020* instrument. Prior to the experiments, DFMs were reduced with pure H_2 for 1 h at 400 °C (Ru-DFMs) or 500 °C (Ni-DFMs) in order to obtain a material with similar reduction degree than in the catalytic activity test. After that, the samples were degasified at the same temperature for 90 min. For both groups of DFMs, the adsorption isotherms were recorded at 35 °C varying the pressure between 50 and 450 mmHg. Adsorption stoichiometries of Ni/H = 1 and Ru/H = 1 were assumed [31].

2.7. Transmission electron microscopy (TEM)

The morphology of the DFMs was analysed by transmission electron microscopy (TEM) in a *JEM-1400 Plus* instrument using a voltage of 100 kV. The reduced DFMs were dispersed in distilled water ultrasonically, and the solutions were then dropped on copper grids coated with lacey carbon film.

2.8. CO_2 temperature-programmed desorption (CO_2-TPD)

The CO_2-TPD experiments were carried out on a Micromeritics *AutoChem 2920* instrument coupled to a *HIDEN ANALYTICAL HPR-20 EGA* mass spectrometer. The DFMs (0.1 g) were pre-reduced at 400 °C (Ru-DFMs) or 500 °C (Ni-DFMs) under 5% H_2/Ar flow (1 h) and then cooled down to 50 °C. The adsorption of CO_2 was performed at 50 °C in a flow of 5% CO_2/He (50 cm^3 min^{-1}) for 60 min. After CO_2 adsorption, the samples were treated with He for 90 min and heated at 10 °C min^{-1} up to 1000 °C in flowing He (50 cm^3 min^{-1}).

2.9. Reactor testing

The catalytic activity, of the synthesized DFMs, in the cyclic operation of CO_2 adsorption and hydrogenation to CH_4 was evaluated in a vertical tubular stainless steel reactor. In each experiment, the reactor was loaded with 1 g of DFM with a particle size between 0.3 and 0.5 mm. Prior to the analysis, the DFMs were reduced with a stream composed of

10% H_2/Ar, progressively increasing the temperature from RT to 400 °C (Ru-DFMs) or 500 °C (Ni-DFMs) and maintaining the final temperature for 60 min. During the adsorption period, a stream composed of 10% CO_2/Ar was fed for 1 min, followed by a purge with Ar for 2 min to remove weakly adsorbed CO_2. Next, during the hydrogenation period, a stream consisting of 10% H_2/Ar was fed for 2 min, followed by an Ar purge for 1 min before starting the adsorption period again. The total flow rate was 1200 $cm^3\ min^{-1}$, which corresponds to a space velocity of 45000 h^{-1}. The flue gas composition was continuously measured using the *MultiGas 2030 FT-IR* analyzer for quantitative analysis of CO_2, CH_4, CO and H_2O. The experiments were carried out in the 280–400 °C (Ru-DFMs) or 280–520 °C (Ni-DFMs) temperature ranges. At this point, it is important to note that nickel has a lower intrinsic activity than ruthenium [32]. Therefore to favour kinetics Ni-DFMs operate at higher temperatures compared to those based on ruthenium [12,14]. Hence, as detailed in the aging procedure section, the temperatures at which DFMs were aged, were also different.

The CH_4 and CO productions were calculated by the following expressions:

$$Y_{CH_4}\left(\mu mol\ g^{-1}\right) = \frac{1}{W}\int_0^t F_{CH_4}^{out}(t)dt \tag{2}$$

$$Y_{CO}\left(\mu mol\ g^{-1}\right) = \frac{1}{W}\int_0^t F_{CO}^{out}(t)dt \tag{3}$$

were W is the catalyst weight loaded in the reactor. On the other hand, CH_4 selectivity is determined by relating the CH_4 and CO productions since they were the only detected carbon based products:

$$S_{CH4}(\%) = \frac{Y_{CH_4}}{Y_{CH_4} + Y_{CO}} \times 100 \tag{4}$$

The error in the carbon balance was deduced by the following expression:

$$s_{CB}(\%) = \left(\frac{Y_{CH_4} + Y_{CO}}{stored\ CO_2} - 1\right) \times 100 \tag{5}$$

where the amount of CO_2 stored was calculated from Eq. (6). For that, the amount that leaves the reactor was subtracted from the amount fed. To determine the amount of CO_2 fed, the stream from the feed system was led directly to the analyser. This profile corresponds to the actual CO_2 input that was fed to the reactor.

$$stored\ CO_2\left(\mu mol\ g^{-1}\right) = \frac{1}{W}\int_0^t \left[F_{CO_2}^{in}(t) - F_{CO_2}^{out}(t)\right] dt \tag{6}$$

3. Results and discussion

3.1. Phases Identification and textural properties

Fig. 1 shows the X-ray diffraction spectra of the DFMs after the calcination step, the reduction protocol and the aging process. In general, in all spectra a background belonging to alumina can be seen on which different peaks stand out. Fig. 1a shows the spectra of the calcined DFMs. In all the Ru-DFMs there are three peaks at 28.0, 35.1 and 54.2° 2θ belonging to RuO_2 and in the Ni-DFMs another three peaks at 37.3, 43.4 and 63.0° 2θ belonging to NiO. Furthermore, a peak belonging to $NaNO_3$ appears at 31.9° 2θ (marked with "o") for Na-based DFMs, whereas for the 4Ru-16Ca two peaks belonging to $Ca_6Al_2O_6(NO_3)_6{\cdot}xH_2O$ appear at 11.1 and 18.9° 2θ (marked with "+"). The appearance of $NaNO_3$ peak evidences that this is an intermediate formed from nitrates coming from Ru, Ni and Ca precursors (nitrates) during the calcination step, which in the subsequent reduction step is finally reduced into the Na_2O active sites for adsorption. The detection of peaks assignable to nitrogenous species indicates the presence of residual nitrates that have not been completely decomposed during the calcination step. In general, the intensity of the peaks of the nitrogen species is higher for the Ru-DFMs compared to the Ni-DFMs. Note that calcination temperatures are different for Ru- (400 °C) and Ni-DFMs (550 °C). At this point, a higher calcination temperature achieves a deeper decomposition of the nitrates. Echegoyen et al. [33] obtained similar conclusions in their study of the calcination temperature with Ni-Al and Ni-Cu-Al catalysts.

Fig. 1b shows the diffraction spectra of the reduced DFMs. As expected, there is only one peak at 44.0° 2θ, belonging to metallic ruthenium, in the Ru-DFMs and two peaks at 44.6 and 51.8° 2θ, belonging to metallic nickel, in the Ni-DFMs. No nitrogenous compound or any peak assignable to the adsorbent phases is detected. Therefore, it can be concluded that after the calcination step and the reduction protocol all elements of the DFMs are in the desired oxidation state. In previous work [19], we concluded that, as the calcination temperature increases, the nitrates decompose largely. However, too high calcination temperature, despite achieving complete decomposition of nitrates, penalizes notably the physicochemical properties of DFMs and consequently their activity.

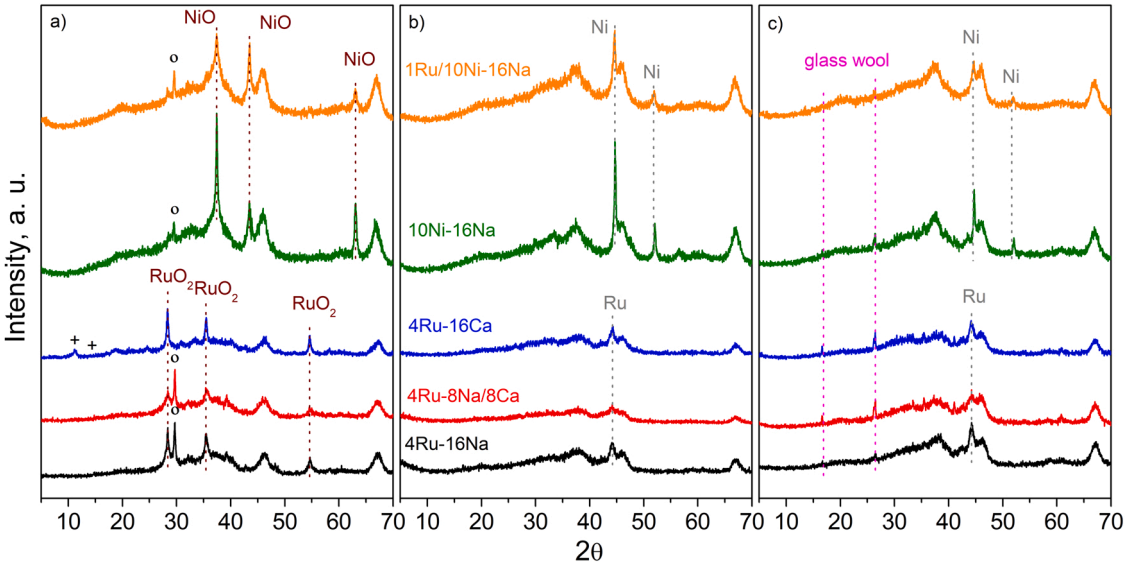

Fig. 1. XRD diffraction spectra of the DFMs: (a) after calcination step, (b) reduction pretreatment and (c) aging process. Diffraction peaks belonging to $Ca_6Al_2O_6(NO_3)_6{\cdot}xH_2O$ are identified with (+) and belonging to $NaNO_3$ with (o).

Table 2
Textural properties of calcined, reduced and aged DFMs.

DFM	S_{BET}, $m^2\ g^{-1}$ calcined DFMs	d_p, Å	V_p, $cm^3\ g^{-1}$	S_{BET}, $m^2\ g^{-1}$ reduced DFMs	d_p, Å	V_p, $cm^3\ g^{-1}$	S_{BET}, $m^2\ g^{-1}$ aged DFMs	d_p, Å	V_p, $cm^3\ g^{-1}$
4Ru-16Na	104.5	125.6	0.341	128.1	134.6	0.444	103.7	143.5	0.384
4Ru-8Na/8Ca	110.6	118.0	0.336	130.6	129.9	0.439	104.8	139.7	0.380
4Ru-16Ca	109.2	107.5	0.304	121.6	121.3	0.382	107.4	129.3	0.360
10Ni-16Na	115.2	115.2	0.404	118.7	147.2	0.462	95.6	173.6	0.425
1Ru/10Ni-16Na	115.6	115.6	0.400	113.0	157.5	0.433	98.0	164.7	0.413

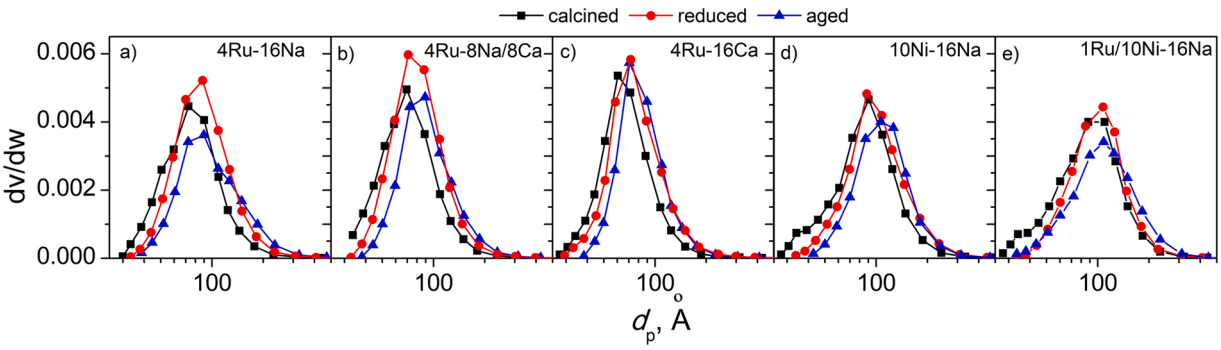

Fig. 2. Pore size distribution of the DFMs: after calcination step, reduction pretreatment and aging process.

In addition, as demonstrated by XRD, even though the calcination step does not decomposed nitrates completely, the reduction protocol does.

The aging process does not modify significantly the X-ray diffraction spectra (Fig. 1c). In all cases the spectra are very similar to those of the reduced DFMs, with the only exception of two peaks belonging to glass wool (17.0 and 26.5° 2θ), which cannot be completely removed after the aging process, since it is used to fix the catalytic bed in the reactor.

Table 2 summarises the values of specific surface area, pore diameter and pore volume for the different DFMs after the calcination step, the reduction protocol and the aging process. Ru-DFMs increase their specific surface after reduction pretreatment (104.5–110.6 vs. 124.6–130.6 $m^2\ g^{-1}$) while Ni-DFMs do not (115.2–115.6 vs. 113.0–118.7 $m^2\ g^{-1}$). This fact is assigned to the different calcination temperatures of the DFMs. A higher calcination temperature decomposes nitrates to a greater extent, as deduced from XRD. In this context, in the calcined Ni-DFMs there is a lower proportion of residual nitrates that are partially or totally blocking the smaller pores. After the reduction protocol, the nitrates decompose completely. At this point, comparing the two families, the reduced Ru-DFMs present a greater specific surface area (121.6–130.6 $m^2\ g^{-1}$) compared to the reduced Ni-DFMs (113.0–118.7 $m^2\ g^{-1}$). This fact is assigned to a minor proportion of alumina in the Ni-DFMs formulation (73–74 vs. 80%) and also due to a certain pore blockage by larger nickel particles, as will be verified in the next section. On the other hand, the pore diameter and pore volume increase in reduced DFMs, confirming the decomposition of residual nitrates observed by XRD. Specifically, the increase in pore volume is significantly greater in the Ru-DFMs, confirming the presence of a greater quantity of residual nitrates.

The aging process causes a reduction in specific surface area and pore volume and an increase in pore size (Table 2). It is suggested that continued exposure of DFMs to temperature in the presence of O_2 and H_2O leads to sintering of the catalytic phase and agglomeration of the adsorbent, which causes irreversible blocking of smaller pores. In order to confirm this aspect, Fig. 2 shows the pore size distributions for the different DFMs after the calcination step (black line), the reduction protocol (red line) and the aging process (blue line). All distributions are unimodal centered around 80–120 Å. As can be observed, the distribution shifts towards higher values with the reduction pretreatment. This fact is ascribed to the elimination of the residual nitrates which partially block the pores. On the other hand, with the aging process, only the beginning of the curve moves towards higher values, while the declines are almost coincident. This fact confirms the total blocking of the small-size pores. Burger et al. [23] observed a progressive decrease in the specific surface area of $NiAl_2O_x$ and $NiFeAl_2O_x$ catalysts as time increased in the operation with continuous feeding of CO_2 and H_2. The authors assigned the decrease to the growth of Ni particles and to sintering of the mixed oxide phase. De-La-Torre et al. [27] also observed a reduction in the specific surface area after hydrothermal aging for Pt-Ba/Al_2O_3 and Pt-Ce-Ba/Al_2O_3 NSR catalysts. The authors assigned the decrease to the formation of barium aluminate and the blocking of the pores of the alumina by platinum and cerium.

Table 3
Ru and Ni dispersion and particle size estimated from TEM micrographs of reduced and aged DFMs.

DFM	D_m, % reduced DFMs	d_c (TEM), nm	D_m, % aged DFMs	d_c (TEM), nm
4Ru-16Na	19.6	8.7	7.4	9.9
4Ru-8Na/8Ca	24.8	6.4	11.3	7.5
4Ru-16Ca	9.8	10.0	4.5	11.7
10Ni-16Na	2.2	11.6	0.9	12.8
1Ru/10Ni-16Na	5.9	10.8	2.1	11.5

3.2. Metallic dispersion

The dispersion of the active phase/s in the DFMs is determined by H_2 chemisorption considering a stoichiometry H/X = 1 (X = Ru or Ni) [31]. Table 3 shows the dispersion values (D_m) of the reduced DFMs. Very different dispersion values are obtained, comprised in the range 2.2–24.8%. The choice of DFMs with such disparate dispersion values allows us deeping into the influence of the aging process on DFMs. In general, different dispersions are obtained depending on whether the DFMs are based on Ru or Ni and depending on the adsorption phases. The discussion about the different dispersion values can be found in previous works [12,14,19,30].

The aging process causes a drastic reduction in the metallic dispersion of DFMs (Table 3). The dispersion values of aged DFMs are comprised in the range 0.9–11.3%, which corresponded to a reduction of 54.1–64.4% compared to the values of the reduced DFMs. Based on

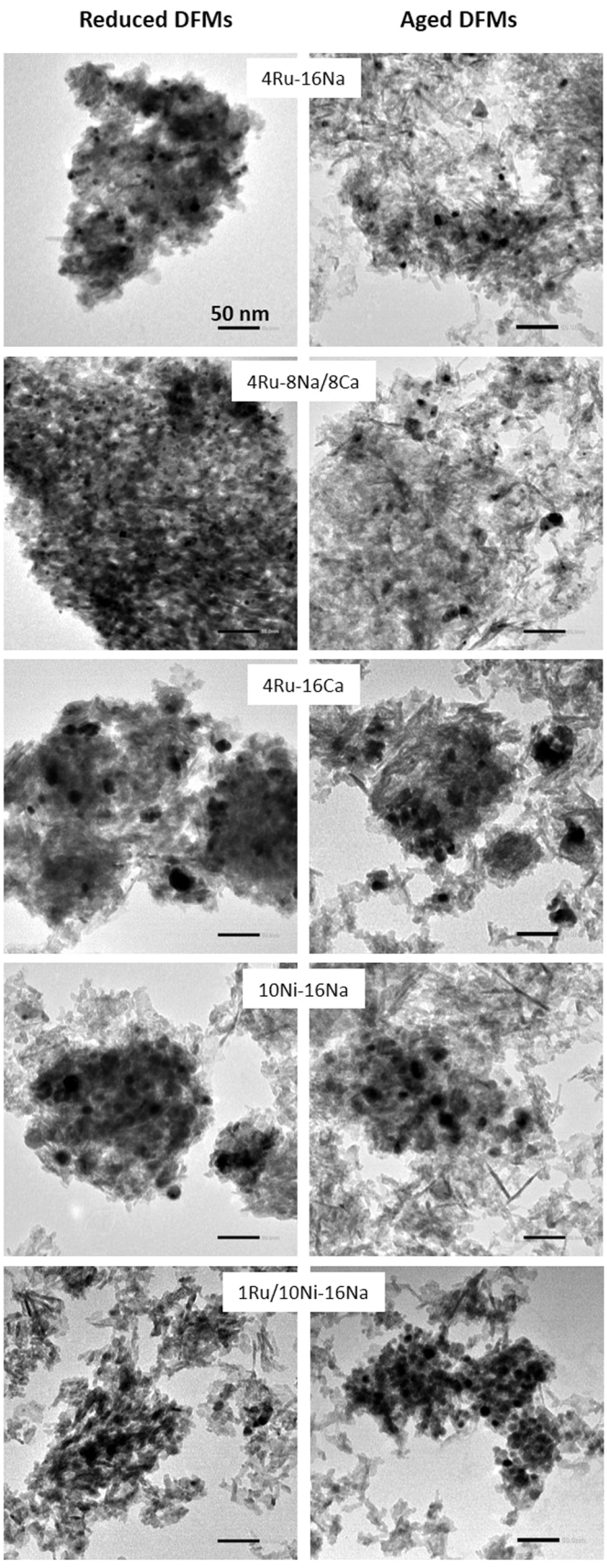

Fig. 3. TEM micrographs of reduced and aged DFMs.

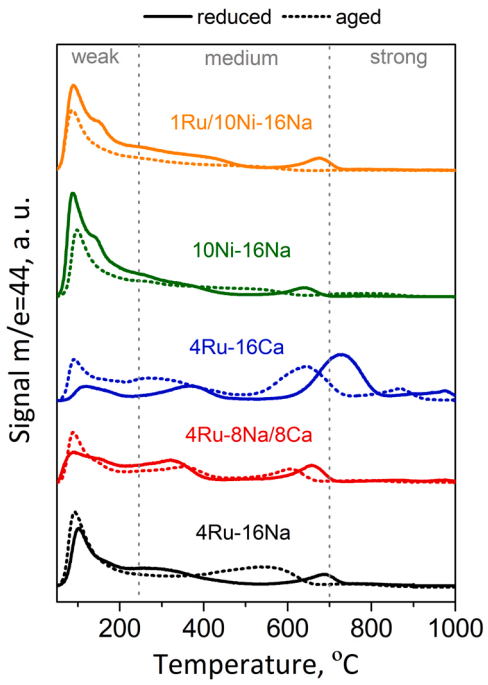

Fig. 4. CO_2-TPD profiles for reduced (continuous line) and aged (dotted line) DFMs.

these results, it can be confirmed that the continued exposure of DFMs to high temperatures in the presence of O_2 and H_2O leads to a sintering of the catalytic phase.

Transmission electron microscopy (TEM) is used to corroborate the sintering of metallic particles after the aging process. Fig. 3 shows the TEM micrographs of the reduced (left column) and aged (right column) DFMs. The darkest areas with circular-shaped in the micrographs correspond to metallic particles. In the case of DFM 1Ru/10Ni-16Na they can correspond to metallic or bimetallic particles of Ni and Ru [19,34,35]. At this point, the average particle size of the metallic or bimetallic particles is estimated by measuring at least 100 particles and the results are collected in Table 3. The histograms of the distribution of the metallic particles of the reduced and aged DFMs are been shown in the supplementary material (Fig. S1). In general, the particle sizes obtained are similar to that determined by H_2-chemisorption. De-La-Torre et al. [27] also observed a considerable reduction in platinum dispersion after hydrothermal aging process for Pt-Ba/Al_2O_3 and Pt-Ce-Ba/Al_2O_3 NSR catalysts. The reduction in dispersion was assigned to the sintering of the metallic phase.

3.3. *Temperature programmed desorption of CO_2 (CO_2-TPD)*

The basicity of DFMs is determined by CO_2 desorption experiments at programmed temperature. Samples were first saturated with a 5% CO_2/Ar mixture, and then purged in an inert atmosphere, and finally a temperature controlled ramp was applied in He. During the temperature ramp, the intensity of signal 44 is monitored with a mass spectrometer. Fig. 4 shows the evolution of the CO_2 signal as a function of temperature during the CO_2-TPD experiments for the reduced (solid line) and aged (dotted line) DFMs. Depending on the desorption temperature, weak, medium and strong basic sites are distinguished. Weak basic sites are unstable and easily decompose below 250 °C. Medium strength basic sites decompose between 250 and 700 °C and strong basic sites are highly stable and do not decompose until 700 °C. All DFMs studied show weak and medium basicity, while only DFM 4Ru-16Ca shows strong basicity. This fact indicates that the strength of calcium carbonates is higher compared to sodium carbonates. A more in-depth analysis of the

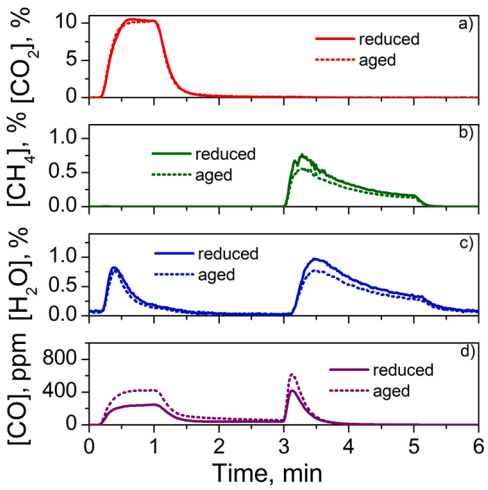

Fig. 5. CO_2, CH_4, H_2O and CO concentration profiles during one cycle of CO_2 adsorption and hydrogenation to CH_4 for the reduced and aged Ru-8Na/8Ca operating at 400 °C.

Table 4
Proposed reactions in each period.

Adsorption period	Eq.	Hydrogenation period	Eq.
$Na_2O+CO_2 \leftrightarrows Na_2CO_3$	(7)	$Na_2CO_3 \leftrightarrows Na_2O+CO_2$	(11)
$CaO+CO_2 \leftrightarrows CaCO_3$	(8)	$CaCO_3 \leftrightarrows CaO+CO_2$	(12)
$2NaOH+CO_2 \leftrightarrows Na_2CO_3+H_2O$	(9)	$CO_2 + 4\,H_2 \leftrightarrows CH_4 + 2\,H_2O$	(1)
$Ca(OH)_2+CO_2 \leftrightarrows CaCO_3+H_2O$	(10)	$CaO+H_2O \leftrightarrows Ca(OH)_2$	(13)
		$Na_2O+H_2O \leftrightarrows 2NaOH$	(14)

different types of basicity depending on the phase or phases of the adsorbent can be found in own previous works [12,14,19,30].

If the profiles of the reduced samples and the aged samples are compared, both follow a similar evolution. On the one hand, the CO_2 desorption for aged Ru-DFMs shifts towards lower temperatures compared to reduced counterparts. On the other hand, the desorption profiles of aged Ni-DFMs present a lower intensity than the reduced counterparts. At this point, it must be taken into account that the aging temperature is different, 400 °C for Ru-DFMs and 550 °C for Ni-DFMs. Furthermore, also the metallic contents are different, 4% for the Ru-DFMs and 10–11% for the Ni-DFMs. The aging process for the Ni-DFMs causes greater coverage of the adsorbent by larger nickel loading. On the other hand, given the lower metallic loading of Ru a lower proportion of the adsorbent phases are covered. Therefore, aging causes agglomeration of the adsorbent and consequently desorption of CO_2 at lower temperatures.

3.4. *Catalytic activity in cycles of CO_2 adsorption and hydrogenation to CH_4*

The catalytic activity is evaluated in cycles of CO_2 adsorption and hydrogenation to CH_4. Fig. 5 shows a complete cycle for the reduced and aged DFM 4Ru-8Na/8Ca at 400 °C. The cycles have a total duration of six minutes. First, it begins with the adsorption period by introducing a stream of 10% CO_2/Ar for one minute, followed by a two-minute purge. Then, the hydrogenation period begins by introducing a stream of 10% H_2/Ar for two minutes. Finally, the global cycle ends with an additional one-minute purge. The detailed description of the temporal evolution of reagents and products, as well as the mechanism, can be found in own previous works [12,14]. Table 4 summarizes the chemical reactions proposed in each period for DFMs based on sodium, calcium or both.

In the adsorption period, the CO_2 is adsorbed, forming carbonates. CO_2 can be adsorbed on oxide sites (Eq. 7 and Eq. 8) or on hydroxide sites (Eq. 9 and Eq. 10). On the other hand, in the hydrogenation period,

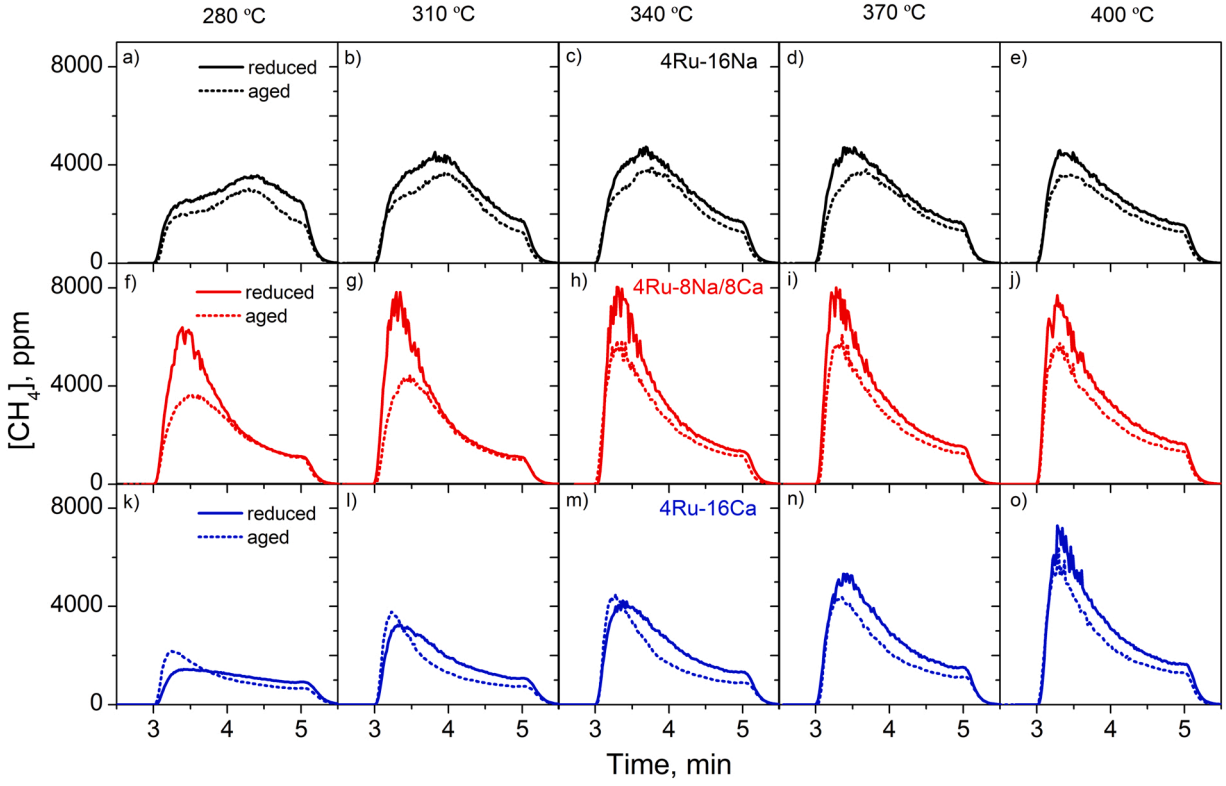

Fig. 6. CH_4 concentration profiles during the hydrogenation period for reduced (continuous line) and aged (dotted line) Ru-DFMs operating at different temperatures (280–400 °C).

the carbonates decompose due to the presence of hydrogen (Eq. 11 and Eq. 12), the desorbed CO_2 is hydrogenated to CH_4 (Eq. 1) and part of the produced water remains adsorbed, forming hydroxides (Eq. 13 and Eq. 14). If the evolution of the reagents and products between the reduced and aged DFM is compared, it can be seen that both follow a very similar evolution with small differences in intensity. Therefore, it is concluded that the aging process does not modify the previously proposed mechanism. Fig. S2 shows a complete cycle for the reduced and aged DFM 10Ni-16Na at 400 °C. The previously proposed mechanism is also valid for reduced and aged Ni-DFMs.

The CO_2 adsorption and hydrogenation cycles to CH_4 have been carried out at different temperature ranges for Ru-DFMs and Ni-DFMs. Note again that, given the lower intrinsic activity of nickel compared to ruthenium, Ni-DFMs commonly operate at higher temperatures. Therefore, the samples have been aged at different temperatures, 400 °C (Ru-DFMs) and 550 °C (Ni-DFMs). Hence, the influence of the aging protocol is studied independently for Ru- and Ni-DFMs in the following sections.

3.4.1. *Catalytic activity of reduced and aged Ru-DFMs*

Fig. 6 shows the evolution of CH_4 concentrations profiles during the hydrogenation period for the reduced (solid line) and aged (dotted line) Ru-DFMs in the temperature range 280–400 °C. In all cases, CH_4 production begins at minute 3 of the cycle that is immediately after the H_2 admission, in correlation with cycle timings shown in Fig. 5. Consequently, the decomposition of carbonates (Eq. 11 and Eq. 12) and their subsequent hydrogenation (Eq. 1) is an instantaneous process with the change of the feed to 10% H_2/Ar. Comparing the DFMs with each other, different evolutions and different trends are observed with the increase in operating temperature. In general, the DFMs 4Ru-16Na (Fig. 6a-e) and 4Ru-8Na/8Ca (Fig. 6f-j) show little variability in CH_4 concentration evolution with increasing operating temperature. On the other hand, DFM 4Ru-16Ca (Fig. 6k-o) clearly modifies its CH_4 concentration evolution with operating temperature. These results are consistent with the different strength of basic sites. The DFM 4Ru-16Ca is the only formulation that presents strong basic sites (Fig. 4), therefore more quantity of CO_2 is available to hydrogenate at high temperature.

Another important aspect to take into account is the CH_4 formation rate. The faster CH_4 forms, the greater the utilization of the H_2 fed. In own previous works [36,37], the CO_2 adsorption and hydrogenation to CH_4 operation has been modeled, simulated and optimized. It was concluded that adsorption times close to DFM saturation and moderate hydrogenation times are optimal, in which there is a compromise between the amount of CH_4 produced and the conversion of H_2 fed. At this point, among the reduced DFMs, the maximum CH_4 concentration for DFM 4Ru-16Na is 4700 ppm at 340 °C, while for DFM 4Ru-16Ca is 7300 ppm at 400 °C. Furthermore, the maximum production for DFM 4Ru-16Ca is detected at earlier hydrogenation times. Consequently, Ca-based DFMs has more favourable CH_4 formation rate than Na-base one for cyclic operation. On the other hand, DFM 4Ru-8Na/8Ca reaches a concentration of 8000 ppm, also in the first moments of the hydrogenation period. At this point, the simultaneous presence of both adsorbents increases the CH_4 formation rate which contributes to improve the compromise between the amount of CH_4 produced and the H_2 conversion.

Comparing the evolutions of the reduced and aged DFMs, in general, they follow the same trend, the concentration of CH_4 for the aged DFMs being slightly lower. However, for DFM 4Ru-16Ca when operating at low temperatures (280–340 °C) the CH_4 concentration of the aged DFM is higher in the early seconds of the hydrogenation period. This fact is due to the adsorbent agglomeration caused by the aging process. As observed in CO_2-TPD experiments (Fig. 4) this favours the desorption of higher amount of CO_2 at lower temperature for aged 4Ru-16Ca.

Fig. 7a shows the evolution of CH_4 production for the reduced and aged Ru-DFMs. The CH_4 productions are obtained from the direct integration of the profiles shown in Fig. 6 aplying Eq. (2). To check the

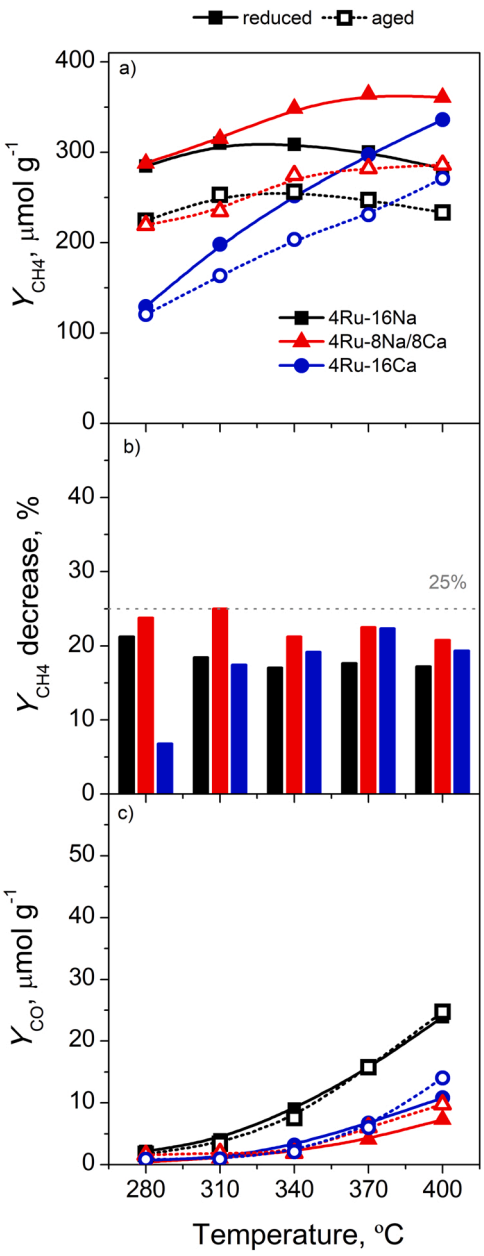

Fig. 7. Evolution of CH_4 (a) and CO (c) productions with temperature for reduced (continuous line and filled markers) and aged (dotted line and hollow markers) together with the percentage of CH_4 production decrease (b) for aged Ru-DFMs.

reliability of the data, the error, with which the carbon balance is closed is determined (Eq. 5). In all cases, it is possible to close the carbon balance with an error below 5%. The DFM 4Ru-16Ca shows an upward trend with operating temperature and the DFMs 4Ru-16Na and 4Ru-8Na/8Ca show less variability. At this point, the DFM composed of both adsorbents (4Ru-8Na/8Ca) presents the highest CH_4 production in the entire temperature range studied. In agreement with that reported in a previous work [30], the modification of the Na_2CO_3/CaO ratio modulates the basicity of DFM (Fig. 4) and improves the dispersion of the metallic phase (Table 3). Consequently, these aspects promote the CO_2 adsorption and hydrogenation to CH_4.

The CH_4 productions of the aged DFMs (hollow symbols linked by dotted lines) decrease with respect to reduced DFMs. Therefore, it is confirmed that exposure to temperature with a stream composed of O_2 and H_2O limits the activity of DFMs. This limitation, as mentioned

above, is caused by the decrease in dispersion due to sintering of the active phase (Table 3) and the agglomeration of the adsorbent. Even so, DFMs composed of a single adsorbent, 4Ru-16Na and 4Ru-16Ca, produce 256 μmol g^{-1} at 340 °C and 271 μmol g^{-1} at 400 °C, respectively. On the other hand, DFM containing both adsorbents (4Ru-8Na/8Ca) produces 286 μmol g^{-1} at 400 °C and in the temperature range 340–400 °C the production does not fall below 275 μmol g^{-1}. At this point, DFM 4Ru-8Na/8Ca is proposed as the most active after the hydrothermal aging in the presence of oxygen. However, the higher activity is not due to a better resistance to aging, but to the higher activity of the reduced DFM. The three Ru-DFMs present a similar aging resistance. For an easier interpretation. Fig. 7b shows the percentages of decrease in the CH_4 production of the aged Ru-DFMs with respect to the reduced at the different operating temperatures. Remarkably, no decrease of methane production higher than 25% is observed. In general, the reduction values are between 17% and 25%, with the exception of DFM 4Ru-16Ca at 280 °C which reduction in only 7%. As previously suggested, the agglomeration of the adsorbent leads to desorption of CO_2 at lower temperatures, which contributes to maintain the production at similar level for this DFM.

Fig. 7c shows the evolution of CO production for reduced and aged Ru-DFMs. In all cases, an upward trend is obtained with temperature and the aging process does not modify the quantity produced. All Ru-DFMs are highly selective to CH_4, in all cases, the selectivity is above 90% (Eq. 4). Furthermore, in DFMs with Ca, the selectivity is above 95%. Previous studies carried out by other authors [38,39], or by ourselves [12,14], reported that the presence of Ca favours the selectivity to CH_4 while the presence of Na favours the formation of CO.

Based on the results of Ru-DFMs, it can be concluded that although the aging process limits the textural properties; considerably high CH_4 productions are still obtained. The fact that all Ru-DFMs studied are highly resistant to aging indicates the possibility of operating for long periods.

3.4.2. *Catalytic activity of reduced and aged Ni-DFMs*

Fig. 8 shows the evolutions of the CH_4 concentrations of the reduced and aged Ni-DFMs at different operating temperatures. For both reduced DFMs a strong dependence on the operating temperature is appreciated. At low temperatures (280 °C) the maximum CH_4 concentration is limited. Subsequently, it increases markedly at moderate temperatures (360–440 °C), and the maximum CH_4 concentration decreases again at higher temperatures (520 °C). On the other hand, comparing the DFMs with each other, it is clearly observed that the promotion of Ni-DFM with small amount of Ru (1% wt.) boosts the CH_4 production. Furthermore, Ru-promoted Ni-DFM (1Ru/10Ni-16Na) exhibits significantly faster CH_4 formation rate. In the previous sections of characterization, the Ru-promotion of a Ni-DFM boosted the metallic dispersion. In agreement with higher melting point of Ru relative to Ni, it is suggested that ruthenium acts as a shell protecting from sintering nickel in the nucleus during the calcination step [34]. Besides, the strong interaction between Ni and Ru also prevents nickel nanoparticles from sintering [19,40]. Tsiotsias et al. [41] in their review analysed bimetallic Ni-Based catalysts for CO_2 methanation. They conclude that the insufficient low-temperature activity, low dispersion and reducibility, as well as nanoparticle sintering of Ni-based catalysts can be partly overcome via the introduction of a second transition metal (e.g., Fe, Co) or a noble metal (e.g., Ru, Rh, Pt, Pd and Re). Through Ni-M alloy formation, or the intricate synergy between two adjacent metallic phases, new high-performing and low-cost methanation catalysts can be obtained. Renda et al. [42] and Zeng et al. [43] in their studies also obtained similar conclusions.

Regarding to aged samples, a noticeable decrease in CH_4 concentration can be observed with respect to reduced sample. This limitation is accentuated in the second minute of hydrogenation (minute 4 of the cycle). It is proposed that with the higher metallic loading (10–11%) the aging process modifies the proximity between the adsorbed carbonates and the available metallic sites. In fact, a significant decrease in the dispersion of the metallic phase and the coverage of the adsorbent phase by the metal has been observed for aged DFMs by characterization techniques. Consequently, a significant proportion of carbonates do not have nearby metal sites available for decomposition and hydrogenation.

For a more in-depth interpretation, the profiles in Fig. 8 were integrated (Eq. 2) and the evolution of CH_4 production per cycle with reaction temperature is shown in Fig. 9a. In all cases, it is possible to close the carbon balance with an error below 5% (Eq. 5). Both DFMs present a similar trend with a maximum of CH_4 production at intermediate temperatures (400 °C) as has also been observed in Fig. 8. The reduced DFMs 10Ni-16Na and 1Ru/10Ni-16Na yield 172 and 250 μmol g^{-1}, respectively. On the other hand, analysing the productions of the aged DFMs, a significant decrease is clearly appreciated. For an easier interpretation, Fig. 9b shows the percentages of decrease in the CH_4 production of Ni-DFMs at the different operating temperatures. On this occasion, compared to the Ru-DFMs (Fig. 7b) the decrease is significantly greater. In fact, production is reduced by up to 60% for the DFM 1Ru/10Ni-16Na operating at 280 °C. At this point, keep in mind that nickel-based catalysts or DFMs commonly operate at higher

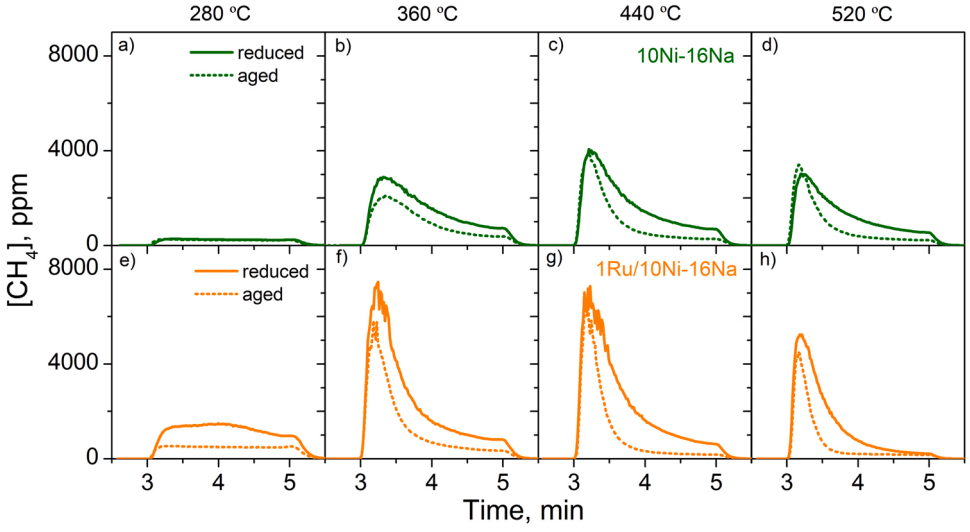

Fig. 8. CH_4 concentration profiles during the hydrogenation period for reduced (continuous line) and aged (dotted line) Ni-DFMs operating at different temperatures (280–520 °C).

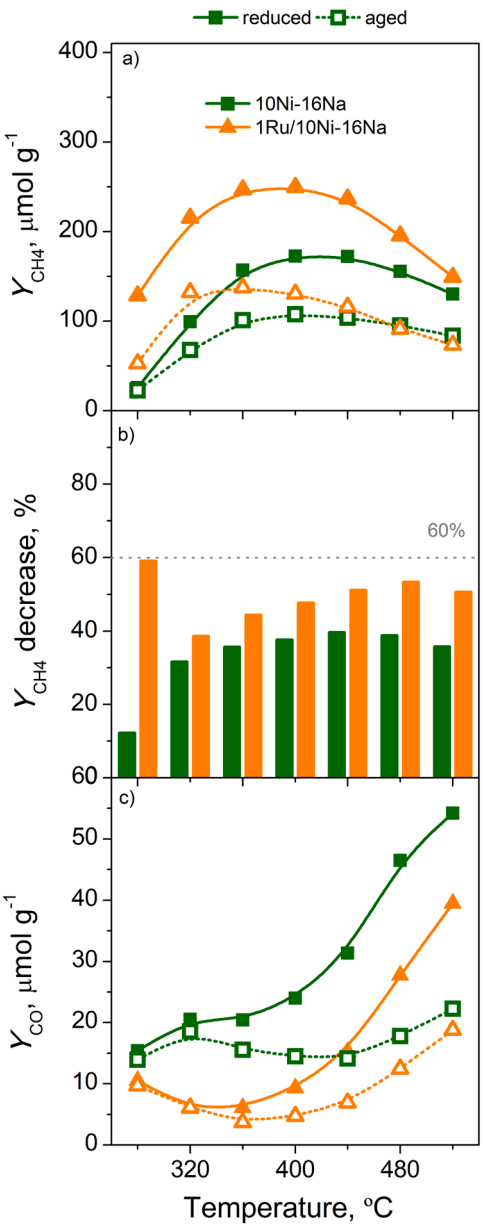

Fig. 9. Evolution of CH_4 (a) and CO (c) productions with temperature for reduced (continuous line and filled markers) and aged (dotted line and hollow markers) together with the percentage of CH_4 production decrease (b) for aged Ni-DFMs.

temperatures than ruthenium-based ones. Therefore, to emulate a long period of operation at a higher temperature, the aging process of Ni-DFMs has been carried out at 550 °C compared to 400 °C of Ru-DFMs. Consequently, the aging process is carried out under more severe conditions in the case of Ni-DFMs.

Comparing both Ni-DFMs with each other, 1Ru/10Ni-16Na shows a greater decrease in CH_4 production at all operating temperatures (Fig. 9b). It is suggested that improvements in the textural properties due to synergistic effects between ruthenium and nickel in the reduced DFM are limited after the aging process. Even so, in general, 1Ru/10Ni-16Na presents a higher CH_4 production in the studied operating temperature range. A production of 137 µmol g^{-1} is obtained at 360 °C for DFM 1Ru/10Ni-16Na and 108 µmol g^{-1} at 400 °C for DFM 10Ni-16Na.

Fig. 9c shows the evolution of CO production of reduced and aged Ni-DFMs. Again, an upward trend is obtained with temperature, however, this time the aging process also decreases the amount of CO produced. DFM 10Ni-16Na exhibits low selectivity to CH_4. In fact, at 400 °C, being

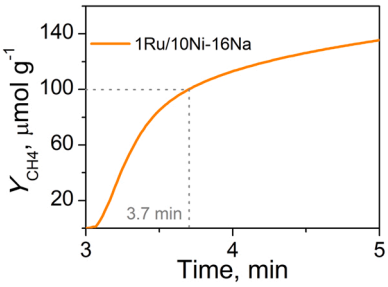

Fig. 10. Cumulative CH_4 production during the hydrogenation period for aged 1Ru/10Ni-16Na at 400 °C.

the temperature at which the CH_4 production and its selectivity is maximized, both for the reduced and for the aged DFMs, the selectivity is 88%. On the other hand, 1Ru/10Ni-16Na presents a selectivity above 95% in the temperature range 320–400 °C, both for reduced and aged DFM.

The ability to produce CH_4 from DFM 1Ru/10Ni-16Na with high selectivity after the aging process stands out. Despite the fact that the textural properties are remarkably diminished and the CH_4 production is remarkably decrease, it is possible to produce 137 µmol g^{-1} at 360 °C with fast CH_4 formation rate. Fig. 10 shows the accumulated methane production with the duration of the hydrogenation period. At 0.7 min (3.7 min of the complete cycle), 100 µmol g^{-1} was produced, confirming the adequate CH_4 formation rate of the aged DFM for the dual process of CO_2 adsorption and hydrogenation to CH_4.

Based on the results of the Ni-DFMs, it can be concluded that aged DFM 1Ru/10Ni-16Na still exhibits acceptable CH_4 production with high selectivity and fast CH_4 formation rate, allowing proper use of hydrogen. However, the DFM 10Ni-16Na has poor catalytic activity after the hydrothermal aging in the presence of oxygen and is therefore not suitable for long periods of operation.

4. Conclusions

Ru/Ni-Na/Ca-Al_2O_3 DFMs with different formulation have been aged, characterised and evaluated in cycles of CO_2 adsorption and hydrogenation to CH_4. The aging process causes a decrease in the textural properties of all DFMs. Furthermore, the dispersion of the metallic phase is also reduced. The continuous exposure of DFMs to temperature in the presence of oxygen and steam causes the sintering of the metallic phase, the agglomeration of the adsorbent phase and the blocking of smaller alumina pores. In Ru-DFMs, adsorbent agglomeration shifts CO_2 desorption at lower temperatures. However, in Ni-DFMs CO_2 desorption is decreased after the aging process. This difference is assigned to the greater coverage of the adsorbent phase due to a higher nickel loading (10–11 vs. 4%) and to the higher temperature of the aging process for the Ni-DFMs (550 vs. 400 °C).

In the activity in cycles of CO_2 adsorption and hydrogenation to CH_4, all the aged DFMs show, in the entire temperature range, a lower CH_4 production compared to the reduced DFMs. Consequently, continued exposure of DFMs to temperature in the presence of oxygen and steam also limits activity. However, the decrease in the CH_4 production does not exceed the 25% for Ru-DFMs subjected to aging process. Therefore, despite the fact that the aging process limits the physicochemical properties of Ru-DFMs, considerable CH_4 productions are obtained with adequate CH_4 formation rate. From that it can be concluded, that all Ru-DFMs studied are suitable for long operation periods. Specifically, the aged DFM 4Ru-8Na/8Ca produces 286 µmol g^{-1} at 400 °C. Furthermore, in the range 340–400 °C, the production is above 275 µmol g^{-1} with a selectivity greater than 95%. As the decrease in CH_4 production after the aging process is comparable for all Ru-DFMs, 4Ru-8Na/Ca is proposed as the best alternative given the higher activity of the reduced DFM.

The catalytic activity in Ni-DFMs is considerably reduced after the aging process. CH_4 production is limited, especially in the second minute of the hydrogenation period. It is proposed that given the higher metallic loading (10–11%), the aging process limits the proximity between the carbonates and the metallic sites. The aged DFM 1Ru/10Ni-16Na produces 137 μmol g^{-1} at 360 °C with a selectivity greater than 95%. Furthermore, in the first 0.7 min of the hydrogenation period, 100 μmol g^{-1} are produced. Therefore, it can be concluded that despite the fact that the aging process considerably decreases the physicochemical properties and the activity, the DFM 1Ru/10Ni-16Na continues to present acceptable CH_4 production with adequate CH_4 formation rate for the dual operation of CO_2 adsorption and hydrogenation to CH_4. The higher CH_4 production of the aged DFM is due to the higher activity of the reduced DFM. Nevertheless, 10Ni-16Na DFM is not suitable for long periods of operation due to its poor catalytic activity after the hydrothermal aging in the presence of oxygen.

CRediT authorship contribution statement

Alejandro Bermejo-López: Validation, Methodology, Investigation, Writing – original draft. **Beñat Pereda-Ayo:** Conceptualization, Methodology, Visualization, Writing – review & editing. **Jon A. Onrubia-Calvo:** Methodology, Visualization, Writing – review & editing. **José A. González- Marcos:** Methodology, Data curation, Supervision, Funding acquisition. **Juan R. González-Velasco:** Conceptualization, Supervision, Project administration, Funding acquisition.

Declaration of Competing Interest

The authors declare that they have no known competing financial interests or personal relationships that could have appeared to influence the work reported in this paper.

Acknowledgements

The financial support from the Science and Innovation Spanish Ministry (PID2019-105960RB-C21) and the Basque Government (IT1297-19) is acknowledged. The authors thank for technical and human support provided by SGIker (UPV/EHU Advanced Research Facilities/ ERDF, EU). One of the authors (JAOC) acknowledges the postdoctoral research grant (DOCREC20/49) provided by the University of the Basque Country.

Appendix A. Supporting information

Supplementary data associated with this article can be found in the online version at doi:10.1016/j.jece.2022.107951.

References

[1] A.F. Hof, K. Esmeijer, H.S. de Boer, V. Daioglou, J.C. Doelman, M.G.J. den Elzen, D. E.H.J. Gernaat, D.P. van Vuuren, Regional energy diversity and sovereignty in different 2 °C and 1.5 °C pathways, Energy 239 (2022), 122197.
[2] N. Höhne, M. den Elzen, J. Rogelj, B. Metz, T. Fransen, T. Kuramochi, A. Olhoff, J. Alcamo, H. Winkler, S. Fu, M. Schaeffer, R. Schaeffer, G.P. Peters, S. Maxwell, N. K. Dubash, Emissions: world has four times the work or one-third of the time, Nature 579 (2020) 25–28.
[3] O. Khalifa, I.I.I. Alkhatib, D. Bahamon, A. Alhajaj, M.R.M. Abu-Zahra, L.F. Vega, Modifying absorption process configurations to improve their performance for Post-Combustion CO_2 capture – what have we learned and what is still Missing? Chem. Eng. J. 430 (2022), 133096.
[4] M.A. Sabri, S. Al Jitan, D. Bahamon, L.F. Vega, G. Palmisano, Current and future perspectives on catalytic-based integrated carbon capture and utilization, Sci. Total Environ. 790 (2021), 148081.
[5] A. Rafiee, K.R. Khalilpour, D. Milani, Chapter 8 - CO_2 conversion and utilization pathways, in: K.R. Khalilpour (Ed.), Polygeneration with Polystorage for Chemical and Energy Hubs, Academic Press, 2019, pp. 213–245.
[6] A. Rafiee, K. Rajab Khalilpour, D. Milani, M. Panahi, Trends in CO_2 conversion and utilization: a review from process systems perspective, J. Environ. Chem. Eng. 6 (2018) 5771–5794.
[7] S. Sun, H. Sun, P.T. Williams, C. Wu, Recent advances in integrated CO_2 capture and utilization: a review, Sust. Energ. Fuels 5 (2021) 4546–4559.
[8] M.S. Duyar, M.A.A. Treviño, R.J. Farrauto, Dual function materials for CO_2 capture and conversion using renewable H_2, Appl. Catal. B: Environ. 168 169 (2015) 370–376.
[9] A.I. Tsiotsias, N.D. Charisiou, I.V. Yentekakis, M.A. Goula, The role of alkali and alkaline earth metals in the CO_2 methanation reaction and the combined capture and methanation of CO_2, Catalysts 10 (2020) 7.
[10] P. Melo Bravo, D.P. Debecker, Combining CO_2 capture and catalytic conversion to methane, Waste Disp. Sust. Energy 1 (2019) 53–65.
[11] I.S. Omodolor, H.O. Otor, J.A. Andonegui, B.J. Allen, A. Alba-Rubio, Dual-function materials for CO_2 capture and conversion: a review, Ind. Eng. Chem. Res. 59 (2020) 17612–17631.
[12] A. Bermejo-López, B. Pereda-Ayo, J.A. González-Marcos, J.R. González-Velasco, Mechanism of the CO_2 storage and in situ hydrogenation to CH_4. Temperature and adsorbent loading effects over Ru-CaO/Al_2O_3 and Ru-Na_2CO_3/Al_2O_3 catalysts, Appl. Catal. B: Environ. 256 (2019), 117845.
[13] S. Cimino, F. Boccia, L. Lisi, Effect of alkali promoters (Li, Na, K) on the performance of Ru/Al_2O_3 catalysts for CO_2 capture and hydrogenation to methane, J. CO_2 Util. 37 (2020) 195–203.
[14] A. Bermejo-López, B. Pereda-Ayo, J.A. González-Marcos, J.R. González-Velasco, Ni loading effects on dual function materials for capture and in-situ conversion of CO_2 to CH_4 using CaO or Na_2CO_3, J. CO_2 Util. 34 (2019) 576–587.
[15] A. Porta, R. Matarrese, C.G. Visconti, L. Castoldi, L. Lietti, Storage material effects on the performance of Ru-based CO_2 capture and methanation dual functioning materials, Ind. Eng. Chem. Res. 60 (2021) 6706–6718.
[16] Z. Zhou, N. Sun, B. Wang, Z. Han, S. Cao, D. Hu, T. Zhu, Q. Shen, W. Wei, 2D-layered Ni–MgO–Al_2O_3 nanosheets for integrated capture and methanation of CO_2, ChemSusChem 13 (2020) 360–368.
[17] F. Kosaka, Y. Liu, S. Chen, T. Mochizuki, H. Takagi, A. Urakawa, K. Kuramoto, Enhanced activity of integrated CO2 capture and reduction to CH4 under pressurized conditions toward atmospheric CO_2 utilization, ACS Sustain. Chem. Eng. 9 (2021) 3452–3463.
[18] S. Cimino, R. Russo, L. Lisi, Insights into the cyclic CO_2 capture and catalytic methanation over highly performing Li-Ru/Al_2O_3 dual function materials, Chem. Eng. J. 428 (2022), 131275.
[19] A. Bermejo-López, B. Pereda-Ayo, J.A. González-Marcos, J.R. González-Velasco, Alternate cycles of CO_2 storage andin situhydrogenation to CH_4 on Ni-Na_2CO_3/Al_2O_3: influence of promoter addition and calcination temperature, Sust. Energ. Fuels 5 (2021) 1194–1210.
[20] M.S. Duyar, S. Wang, M.A. Arellano-Treviño, R.J. Farrauto, CO_2 utilization with a novel dual function material (DFM) for capture and catalytic conversion to synthetic natural gas: an update, J. CO2 Util. 15 (2016) 65–71.
[21] M.A. Arellano-Treviño, Z. He, M.C. Libby, R.J. Farrauto, Catalysts and adsorbents for CO_2 capture and conversion with dual function materials: limitations of Ni-containing DFMs for flue gas applications, J. CO2 Util. 31 (2019) 143–151.
[22] H.L. Huynh, W.M. Tucho, Q. Shen, Z. Yu, Bed packing configuration and hot-spot utilization for low-temperature CO_2 methanation on monolithic reactor, Chem. Eng. J. 428 (2022), 131106.
[23] T. Burger, S. Ewald, A. Niederdränk, F.E. Wagner, K. Köhler, O. Hinrichsen, Enhanced activity of co-precipitated $NiFeAlO_x$ in CO_2 methanation by segregation and oxidation of Fe, Appl. Catal. A Gen. 604 (2020), 117778.
[24] Q. Zheng, R. Farrauto, A. Chau Nguyen, Adsorption and methanation of flue Gas CO_2 with dual functional catalytic materials: a parametric study, Ind. Eng. Chem. Res. 55 (2016) 6768–6776.
[25] S. Wang, R.J. Farrauto, S. Karp, J.H. Jeon, E.T. Schrunk, Parametric, cyclic aging and characterization studies for CO_2 capture from flue gas and catalytic conversion to synthetic natural gas using a dual functional material (DFM), J. CO_2 Util. 27 (2018) 390–397.
[26] M.A. Arellano-Treviño, N. Kanani, C.W. Jeong-Potter, R.J. Farrauto, Bimetallic catalysts for CO_2 capture and hydrogenation at simulated flue gas conditions, Chem. Eng. J. 375 (2019), 121953.
[27] U. De-La-Torre, B. Pereda-Ayo, J.A. Onrubia, J.R. González-Velasco, Effect of the presence of ceria in the NSR catalyst on the hydrothermal resistance and global DeNO_x performance of coupled LNT–SCR systems, Top. Catal. 61 (2018) 1993–2006.
[28] C. Seo, H. Kim, B. Choi, M.T. Lim, C. Lee, C. Lee, De-NO_x characteristics of a combined system of LNT and SCR catalysts according to hydrothermal aging and sulfur poisoning, Catal. Today 164 (2011) 507–514.
[29] J. Wang, Y. Ji, G. Jacobs, S. Jones, D.J. Kim, M. Crocker, Effect of aging on NO_x reduction in coupled LNT–SCR systems, Appl. Catal. B: Environ. 148 149 (2014) 51–61.
[30] A. Bermejo-López, B. Pereda-Ayo, J.A. Onrubia-Calvo, J.A. González-Marcos, J. R. González-Velasco, Tuning basicity of dual function materials widens operation temperature window for efficient CO_2 adsorption and hydrogenation to CH_4, J. CO_2 Util. 58 (2022), 101922.
[31] E. Miyazaki, Chemisorption of diatomic molecules (H_2, N_2, CO) on transition d-metals, J. Catal. 65 (1980) 84–94.
[32] A. Quindimil, U. De-La-Torre, B. Pereda-Ayo, A. Davó-Quiñonero, E. Bailón-García, D. Lozano-Castelló, J.A. González-Marcos, A. Bueno-López, J.R. González-Velasco, Effect of metal loading on the CO_2 methanation: a comparison between alumina supported Ni and Ru catalysts, Catal. Today 356 (2019) 419–432.
[33] Y. Echegoyen, I. Suelves, M.J. Lázaro, R. Moliner, J.M. Palacios, Hydrogen production by thermocatalytic decomposition of methane over Ni-Al and Ni-Cu-Al catalysts: effect of calcination temperature, J. Power Sources 169 (2007) 150–157.

[34] S. Li, D. Gong, H. Tang, Z. Ma, Z. Liu, Y. Liu, Preparation of bimetallic Ni@Ru nanoparticles supported on SiO_2 and their catalytic performance for CO methanation, Chem. Eng. J. 334 (2018) 2167–2178.
[35] G. Zhou, Y. Dong, D. He, Bimetallic Ru–M/TiO2 (M = Fe, Ni, Cu, Co) nanocomposite catalysts facribated by galvanic replacement: structural elucidation and catalytic behavior in benzene selective hydrogenation, Appl. Surf. Sci. 456 (2018) 1004–1013.
[36] A. Bermejo-López, B. Pereda-Ayo, J.A. González-Marcos, J.R. González-Velasco, Modeling the CO_2 capture and in situ conversion to CH_4 on dual function Ru-Na_2CO_3/Al_2O_3 catalyst, J. CO_2 Util. 42 (2020), 101351.
[37] A. Bermejo-López, B. Pereda-Ayo, J.A. González-Marcos, J.R. González-Velasco, Simulation-based optimization of cycle timing for CO_2 capture and hydrogenation with dual function catalyst, Catal. Today (2021).
[38] T.A. Le, T.W. Kim, S.H. Lee, E.D. Park, Effects of Na content in Na/Ni/SiO_2 and Na/Ni/CeO_2 catalysts for CO and CO_2 methanation, Catal. Today 303 (2018) 159–167.
[39] L. Xu, H. Yang, M. Chen, F. Wang, D. Nie, L. Qi, X. Lian, H. Chen, M. Wu, CO_2 methanation over Ca doped ordered mesoporous Ni-Al composite oxide catalysts: the promoting effect of basic modifier, J. CO2 Util. 21 (2017) 200–210.
[40] M. Muñoz, S. Moreno, R. Molina, The effect of the absence of Ni, Co, and Ni–Co catalyst pretreatment on catalytic activity for hydrogen production via oxidative steam reforming of ethanol, Int. J. Hydrog. Energ. 39 (2014) 10074–10089.
[41] A.I. Tsiotsias, N.D. Charisiou, I.V. Yentekakis, M.A. Goula, Bimetallic Ni-based catalysts for CO_2 methanation: a review, Nanomaterials 11 (2021) 28.
[42] S. Renda, A. Ricca, V. Palma, Study of the effect of noble metal promotion in Ni-based catalyst for the Sabatier reaction, Int. J. Hydrog. Energ. 46 (2021) 12117–12127.
[43] W. Zhen, B. Li, G. Lu, J. Ma, Enhancing catalytic activity and stability for CO_2 methanation on Ni–Ru/γ-Al_2O_3 via modulating impregnation sequence and controlling surface active species, RSC Adv. 4 (2014) 16472–16479.